PHOTOINDUCED TWO-NUCLEON EMISSION IN NEAR SUPER-PARALLEL KINEMATICS

I.J.D. MacGregor[1,*]

(FOR THE PIP-TOF GROUP OF THE MAINZ A2 COLLABORATION)

[1] *Department of Physics and Astronomy, University of Glasgow, Glasgow G12 8QQ, Scotland, UK*

Electromagnetically induced two-nucleon emission reactions are sensitive to the interaction between nucleon pairs in the target nucleus. Contributing mechanisms include Meson Exchange Currents (MEC), Δ-currents, Final State Interactions (FSI) and Nucleon-Nucleon Correlations (NNCOR). The roles of MEC and Δ-currents in two-nucleon emission reactions are well established. The task now confronting experimenters is to devise experiments which are sensitive to the interesting NNCOR, while minimising the effects of other contributions. This paper reports experiments carried out to measure (γ,NN) cross sections on ^{4}He and ^{16}O in near super-parallel kinematics where NNCOR are expected to be relatively large and the contribution from Δ-currents is suppressed. By measuring at photon energies above the Δ-resonance the influence of Δ-currents is further reduced. Complementary information is obtained from the (γ,pn) and (γ,pp) reactions. The former reaction is sensitive to Tensor Correlations (TenCOR) which are absent in (γ,pp) , whereas the NNCOR contribution to (γ,pp) comes entirely from central Short Range Correlations (SRC). MEC contributions are also expected to be negligible in this reaction channel. Discrimination against FSI between the emitted nucleons and the residual nucleus is provided by strict cuts on the measured missing energy and FSI between the two outgoing nucleons are negligible for (γ,pp) in these kinematics. The motivation, execution and current state of analysis of the ^{4}He(γ,NN) and ^{16}O(γ,NN) measurements are described.

1. INTRODUCTION AND MOTIVATION

It has long been established that the absorption of photons can provide a clean and useful tool to study the atomic nucleus and its constituent hadrons[1, 2]. Quasifree nucleon knockout becomes important above the nucleon emission threshold energy. In quasifree knockout reactions the mismatch between the momentum of the incoming photon and that of the ejected nucleon is balanced by the initial state momentum of the nucleon. However, as the photon energy is increased the momentum mismatch also increases and single nucleon knockout becomes less probable. For photon energies above ≈100 MeV reactions in which two nucleons are emitted are favoured over single nucleon knockout reactions. In these two-nucleon knockout reactions the energy of the incident photon is shared between the two nucleons and their relative motion absorbs the momentum mismatch. The residual nucleus takes no active part in the interaction and acts purely as a spectator. The study of such two-nucleon emission reactions provides an ideal method of probing the interaction between nucleons in the nucleus.

For reactions in which the photon interacts directly with a nucleon pair the nucleons are emitted at 180° in the centre-of-mass frame of the photon and the pair. However, due to the forward momentum of the photon and the randomly oriented initial momentum of nucleon pair, this angle is generally shifted away from 180° , and smeared out, in the transformation to the laboratory frame. Despite the smearing of the nucleon opening angle, a clear experimental signature of such events is the observation of two nucleons emitted in generally "back-to-back" directions which exhaust nearly all of the available energy.

Cuts on low missing energy serve to filter out reactions where the residual nucleus absorbs energy from the incident photon or where the outgoing nucleons lose energy through Final State Interactions (FSI) with the residual nucleus[3]. This is illustrated in figure 1 which shows missing

*Electronic address: i.macgregor@physics.gla.ac.uk

energy spectra from the ^{12}C(γ,pn) reaction for a range of photon energies up to 700 MeV[4], compared to calculations made with the Valencia model[5].

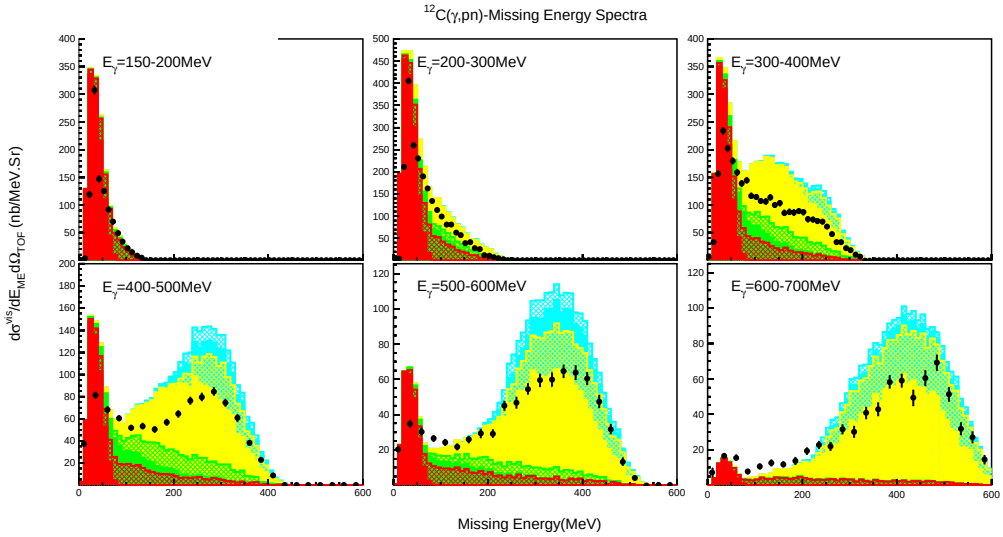

FIG. 1: $^{12}C(\gamma, pn)$ *missing energy spectra[4] compared with the predictions of the Valencia Model[5]. The cross section for each of the eight contributing processes modeled are shown separately. The contributions are stacked in the order 2N, 2N+FSI, 3N, 3N+FSI, Nπ+ABS, Nπ (π emitted), NNπ+ABS, NNπ (π emitted).*

Direct two-nucleon knockout is expected at low missing energies. The observed spectra show a strong peak just above the reaction threshold and this is interpreted as evidence of a direct emission process. Moreover, this peak remains distinct up to the highest photon energies studied, indicating that the direct process can be measured over a very wide range of photon energies.

The Valencia model gives a generally good description of the various processes contributing to two nucleon emission, although at high photon energies some of the direct 2N strength appears to be more smeared out in the data than the model predicts. The model also overestimates the strength of some of the indirect processes at photon energies above ~300 MeV. The smearing of the experimental 2N strength to slightly higher missing energies may be due in part to poorer energy resolution at higher particle energies; an effect which is not included in the model. It may also mean that FSI, which generally shift events to higher missing energies, are stronger than the model predicts. However, the model clearly attributes all of the strength in the low missing energy peak to the direct two-nucleon emission process.

It is clear from the observation of a distinct peak and from the interpretation provided by the Valencia model that cuts on low missing energy will provide a clean sample of the direct two-nucleon emission process. Reactions where either of the outgoing nucleons suffer FSI with the residual nucleus or reactions which share the photon energy with more than two nucleons will be very effectively filtered out by this condition.

The main contributions to direct two-nucleon emission arising from the 1- and 2-body currents[6, 7] are shown in figure 2.

In the Δ-current contribution the photon interacts with a nucleon, exciting it into a Δ state. The Δ subsequently decays emitting a pion which is absorbed on a second nucleon which is then emitted. In the MEC contribution the photon interacts with a nucleon that emits a pion which is absorbed on a second nucleon. This is the so-called pion-seagull mechanism. Alternatively the photon can interact directly with a pion being exchanged between two nucleons. This is the pion-in-flight contribution. The Δ and pion-exchange mechanisms provide most of the direct two-nucleon

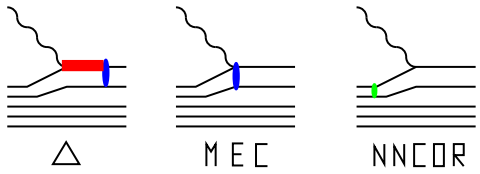

FIG. 2: Mechanisms leading to the direct emission of nucleon pairs include the 2-body Δ- and Meson Exchange Currents (MEC), and initial state nucleon-nucleon correlations (NNCOR) coupled to a 1-body photon interaction.

emission cross section, with smaller contributions arising from the interaction of the photon with a pre-existing Δ in the nucleus and from the exchange of heavier mesons.

Nucleons involved in violent, repulsive and short range interactions can also contribute to direct two-nucleon emission. A photon interacting with a nucleon involved in such a strong nucleon-nucleon correlation (NNCOR) will generally result in both nucleons being emitted.

Single nucleon knockout reactions in which the outgoing nucleon undergoes FSI can also result in the emission of two nucleons. However such FSI generally produce events with high missing energy and/or a wide range of particle opening angles and so will be rejected by a low missing energy cut and by selections on the opening angles of the two emitted nucleons.

It is also possible for the nucleons emitted in any of the direct processes shown in figure 2 to undergo FSI with the residual nucleus. However, the same general considerations apply in this case and such events will be filtered out by the same energy and angular cuts on the experimental data, so while the number of events accepted will be reduced, those that are detected will still be representative of direct processes.

There remains the possibility of FSI in which the two emitted nucleons interact with each other. Such NN-FSI would not affect the total energy and momentum of the pair and so would contribute to the measured data sample. Only recently has this effect been considered in detail for the case of electromagnetically induced two-nucleon emission from nuclear matter [8] and from ^{16}O [9]. In the work on ^{16}O both the mutual interaction between the two nucleons and the interaction of the emitted nucleons with the residual nucleus is taken into account using a perturbative treatment of the optical potential and the NN-interaction, retaining first order terms in the scattering amplitudes. This work has shown that NN-FSI generally increase the (e,e′NN) cross sections, although the size of the effect depends on the reaction kinematics and on the isospin of the pair. The enhancement is usually greater for 2-body currents than the 1-body currents and is also larger for the (e,e′pn) reaction than for (e,e′pp) in the same kinematics.

Calculations have also been carried out for the ^{16}O(γ,pp) reactions in super-parallel kinematics [9]. In these kinematics one nucleon is emitted in the direction of the momentum transfer (photon direction) and the other nucleon in the opposite direction. As discussed in more detail below, the contribution from two-body currents is strongly suppressed under these conditions leaving the dominant contribution from 1-body currents. The calculations show that the effect of NN-FSI is completely negligible under these conditions. The reason is that only the longitudinal component of the 1-body current is sensitive to NN-FSI and this is absent in reactions with real photons, which are purely transverse in character.

The nature of the NNCOR contributions are different in the (γ,pn) and (γ,pp) channels[10]. The (γ,pn) NNCOR are dominated by tensor correlations between nucleon pairs with S=1. These have a much larger contribution to the cross section than the central repulsive short range correlations (SRC) and are felt at nucleon-nucleon separations up to ∼2 fm. In contrast, tensor correlations are absent in the (γ,pp) channel due to isospin reasons[6, 7, 9] and only central SRC contribute. While this channel should provide a clean signal from central SRC the effect of NNCOR will be much weaker than in the (γ,pn) channel. However, to clearly disentangle the various NNCOR effects measurements in both the (γ,pp) and (γ,pn) reaction channels are required.

In order to see the effects of these interesting NNCOR it is necessary to carry out experiments

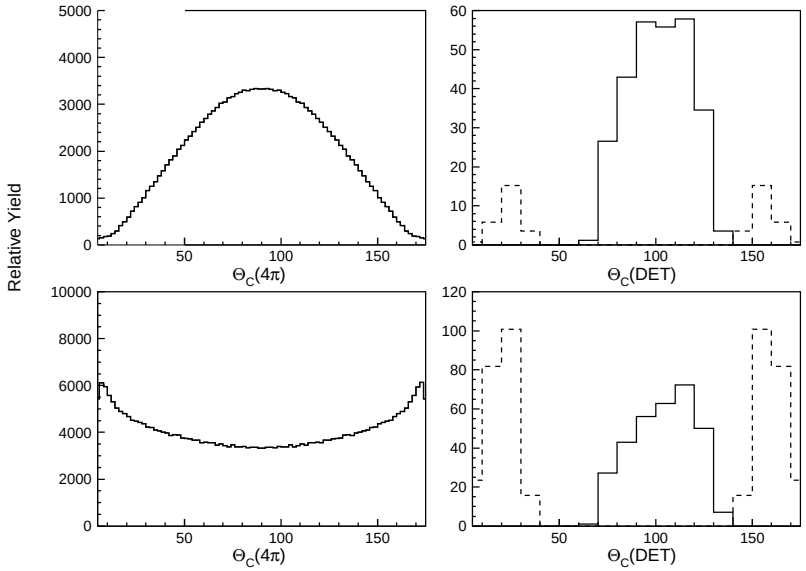

FIG. 3: Differential cross sections as a function of the centre-of-mass angle θ_{CM} for ^{12}C(γ,pp) at E_γ =500 MeV calculated using the Gent factorised model. The top panels show the distributions when only the Δ-current is included. The bottom panels show the predictions including SRC calculated using the FHNC technique. The LH panels show distributions into 4π whereas the RH panels show differential cross sections into the detector geometries of the present experiment. In the RH panels the SOLID lines show the visible cross section in symmetric kinematics whereas the DASHED lines show the cross sections expected in the forward/backward ToF detectors.

in kinematic regions where MEC and Δ- currents are suppressed. Pion exchange is strongly isospin dependent and is suppressed in the (γ,pp) channel. Therefore it should be easier to see NNCOR effects in this channel compared to (γ,pn) .

The photon energy dependence of Δ excitation can be used to suppress contributions from Δ-currents. As seen in figure 1, the measured ^{12}C(γ,pn) cross section for E_m <40 MeV, corresponding to direct two-nucleon emission, is largest in the photon energy range E_γ = 200-300 MeV which reflects the peak of the Δ-resonance excitation. By choosing photon energies either above or below the Δ-resonance, its contribution can be reduced. Two recent (e,e$'$pn) experiments on ^{16}O [11] and ^{3}He [12], carried out by the A1 collaboration at Mainz selected energy transfers below the Δ-resonance. In contrast this experiment focussed on photon energies above the Δ-resonance.

Due to the large width of the Δ-resonance and its associated high and low energy tails, contributions from Δ-currents can still be important at energies well away from the resonance. Some further suppression of Δ-currents can be achieved by exploiting the angular dependence of its excitation.

Calculations using the Gent factorised model[6] of the (γ,pp) reaction were carried out to identify the best kinematic regions to study SRC. While the factorised approach is known to overestimate the effects of central SRC and to underestimate Δ-currents, these calculations provide a valuable indication of the angular dependence of the Δ contribution and the contribution from SRC, and

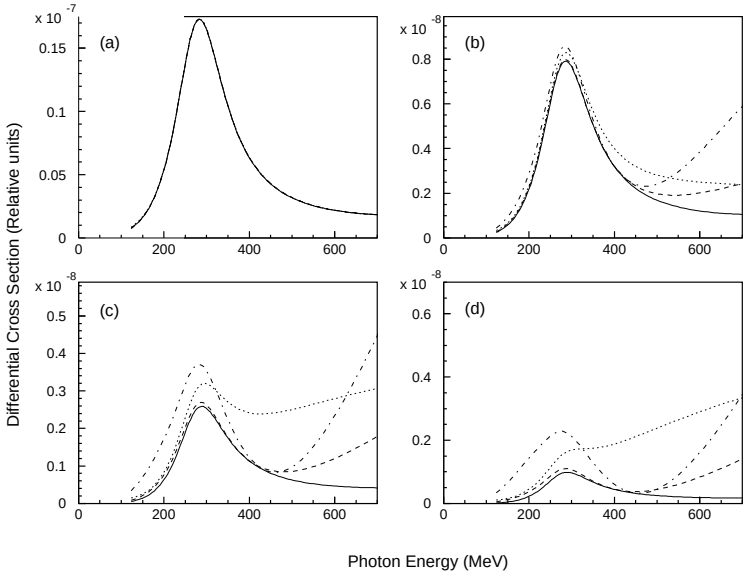

FIG. 4: Calculated E_γ dependence of the (γ,pp) cross section using the factorised Gent model, for events with P=300 MeV/c. The solid line shows the Δ term on its own. The dashed line shows a VMC calculation of SRC. The dotted line shows a FHNC calculation and the dot-dashed is the GD prediction. Panel (a) corresponds to symmetric kinematics (θ_{CM}=90°). Panels (b), (c) and (d) correspond to θ_{CM}=45° , 25° and 15° .

hence are useful in choosing the kinematic regions best suited to study SRC in nuclei.

In this model pions created from the decay of the Δ resonance are predominantly emitted in a direction orthogonal to the direction of momentum transfer defined by the photon beam. Contributions to the (γ,pp) channel from the reabsorption of these pions on a single proton are therefore small at extreme forward and backward angles[6]. In contrast, the effects due to SRC are actually maximised at angles close to the direction of the momentum transfer and also increase with photon energy.

Some results of these calculations are given in figure 3 which shows calculated angular distributions for the emission of $(1p)^2$ protons in the ^{12}C(γ,pp) reaction at E_γ =500 MeV. The figure shows distributions with and without the effects of SRC. The SRC correlation function used here is a central function obtained using the Fermi Hypernetted Chain technique which is currently thought to give a reasonable representation of short range nucleon interactions. At these high photon energies SRC provide a strong enhancement of the cross section at extreme forward and backward angles. The large differences between the Δ currents and SRC are such that the current experiment will be readily able to identify whether or not SRCs contribute significantly to the (γ,pp) channel, as predicted by the calculations.

Figure 4 shows the calculated E_γ dependence of the (γ,pp) cross section using the factorised Gent model [6], for events with a pair momentum of 300 MeV/c, for four different CM angles of the emitted pair and for a wider range of reasonable central SRCs. The SRC effects become more

important as the photon energy increases and the data at forward-backward angles should be able to distinguish at least some of these different possible SRCs. It is also interesting to note that the sensitivity to SRCs vanishes at symmetric angles, θ_{cm}=90° , and this fact may be used to establish the overall strength due to the Δ current on its own.

In practice any measurement will cover a range of angles and so the data will be averaged over a range of kinematic conditions. Fermi motion will also tend to average the effects by smearing the angles involved. However at photon energies around 500 MeV the Fermi cone is relatively narrow (∼20°) and in addition the experiments will measure the recoil momentum and so will allow data to analysed in the centre-of-momentum frame of the incident photon and the nucleon pair.

In the photon energy range E_γ =100-400 MeV the (γ,NN) cross sections are dominated by MEC and Δ-currents. Previous experimental work[3] has shown that in this photon energy range the ^{12}C(γ,pn) and ^{12}C(γ,pp) missing momentum spectra are very well described, up to missing momenta of 400 MeV/c, by the pair momentum distribution F(P), obtained by folding together the momentum wavefunctions of the two ejected nucleons. This result is expected on the basis of simple Plane Wave theoretical treatments of the (γ,NN) reaction, in which the cross section is factorised into the F(P) term, based on the the mean field description of the participating nucleons, and a second factor S_{fi} which contains information on the more interesting short range interactions between the two nucleons. In more sophisticated Distorted Wave theoretical treatments the cross section no longer factorises neatly into these two terms. Nevertheless it has been demonstrated that the factor F(P) still dominates the cross section[6].

Figure 5 shows the initial pair momentum spectra obtained in our previous ^{12}C(γ,pn) wide phase space experiment[4] which sampled kinematics away from the standard quasideuteron back-to-back kinematics. In particular, this experiment was sensitive to regions of very large pair momentum. The data have been divided by the initial pair momentum distribution F(P) and so emphasise differences from the standard mean-field predictions for direct two nucleon emission. There is a systematic enhancement at pair momenta above 400 MeV/c. It is expected that this region may be populated either by NNCOR, or by FSI which do not significantly change the energies of the outgoing nucleons. We also show a calculation by Orlandini and Sarra[13] of the strength expected due to NNCOR in the case of ^{16}O , which accounts for most of the excess data.

The experimental data in figure 5 were divided by an F(P) pair momentum distribution calculated using harmonic oscillator wavefunctions. While these are generally adequate at low momenta, they do not describe large momenta very well. To guage the effects of this the deviations from the harmonic oscillator F(P) obtained using more realistic Hartree Fock or Woods Saxon single particle momentum wave functions were calculated and are also shown in the figure. These also produce variations above pair momenta of 400 MeV/c, but are not sufficient to explain the excess strength observed in the experimental data.

There is a strong indication from this previous work that large pair momenta define a useful region for study where effects of NNCOR may be evident. It is expected that more accurate and extensive data will be obtained at large missing momenta from the analysis of the data from the present experiment.

Two targets, ^{4}He and ^{16}O , were chosen for this experiment. Both are closed shell nuclei: ^{4}He containing only 1s nucleons and ^{16}O having complete 1s and 1p shells. ^{4}He also has the advantage of being a dense nucleus in which the effects of NNCOR might be expected to be enhanced. There is also less scope for FSI in ^{4}He .

In summary the aims of this experiment are to investigate the (γ,NN) reactions in ^{4}He and ^{16}O in regions as close to the photon beam direction as experimentally practical, and in regions of very large missing momenta, for photon energies above the Δ resonance. The experiment concentrates on the (γ,pp) channel, where the effects due to SRC are expected to be easier to disentangle, but also simultaneously measures the (γ,pn) cross section in the same kinematic regions.

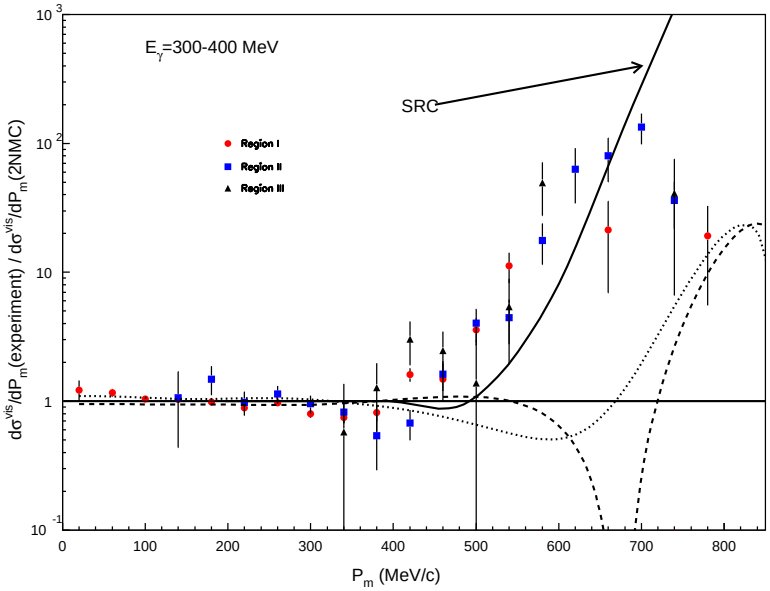

FIG. 5: Ratio of ^{12}C(γ,pn) initial pair momentum data to the calculated F(P) distribution at E_γ =300-400 MeV for E_m $\leq$40 MeV. The three data sets correspond to different kinematic regions. The predicted effects of SRC, calculated for ^{16}O by Orlandini and Sarra[13], are shown in the figure. The dashed (dotted) lines show the deviation from the harmonic oscillator F(P) distribution when using more realistic Hartree-Fock (Woods-Saxon) wavefunctions.

2. EXPERIMENTS

The experiments were performed in Spring 2002 using the Glasgow Tagged Photon facility[14] at the Mainz electron microtron MAMI-B[15]. An electron beam of energy 855 MeV was incident on a 4μm Nickel foil radiator. Bremsstrahlung photons passed through a tungsten collimator, 5mm diameter and 20cm long, to produce a photon beam spot of $\sim$15mm diameter on the target. The residual electrons were momentum analysed in the spectrometer magnetic field before being detected in an array of 352 scintillator detectors mounted on the spectrometer focal plane. The maximum useable counting rate of each of the tagger detectors is $\sim 10^6$ Hz. In order to optimise the rate for reactions in the Δ-resonance and above, those sections of the tagger focal plane detector corresponding to photon energies less than 198 MeV were switched off. The tagged photon energy range was 198 to 793 MeV.

Figure 6 shows a schematic layout of the Glasgow Tagged Photon Spectrometer[14] and the experimental apparatus. The reaction products were detected in five stands of Time-of-Flight (ToF) detectors[16] and in the Proton-Pion Hodoscope PiP[17]. The forward ToF stands (ToF 4 and ToF 5) consist of four layers of scintillator detectors: one thin layer follwed by three thicker layers. Each layer contains eight scintillator bars. The thick bars are 3m high by 20cm wide by 5 cm thick. The thin layers are 1cm thick and overlap each other. The combination of thin and

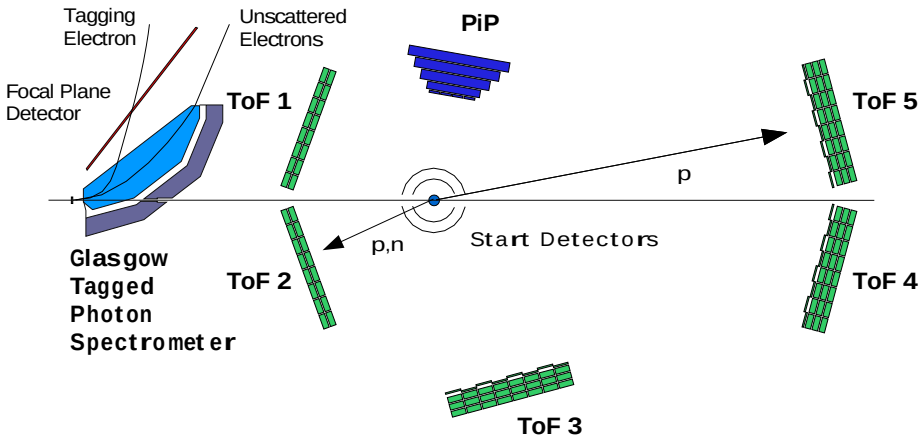

FIG. 6: Schematic diagram of experiment layout.

TABLE I: Positions of detectors.

Detector	Distance (m)	In-plane Angles (degrees)
ToF 1	2.62	-134.5 to - 164.2
ToF 2	2.74	133.7 to 162.7
ToF 3	7.09	72.4 to 60.1
ToF 4	10.44	5.5 to 13.4
ToF 5	10.86	-3.7 to -11.1
PiP	0.88	-42.8 to -91.8

thick layers provides a particle telescope which allows protons, pions, electrons and neutrons to be distinguished. Having three thick layers triples the detection efficiency for neutrons, which is estimated to be ∼5% for each layer, and provides a clean identification of high energy protons. Protons of energies up to ∼250 MeV are stopped in the three layers.

The central ToF (ToF 3) stand also consists of one thin layer and three thick layers. However the two backward ToF stands (ToF 1 and ToF 2) only have two thick layers. As protons emitted in the backward direction are expected to have low energies these stands are placed closer to the target than the forward ToF stands. The forward and backward stands are placed as close to the photon beam line as the raw counting rates in the detector elements will permit. Table 1 gives the distances and in-plane angles of each of the detectors, with the convention that angles on the PiP-side are negative and angles on the side opposite are positive.

Start signals for the ToF detectors were provided by two concentric rings of thin scintillation detectors[19] around the target. The inner ring consists of 14 segments with gaps ±5° at forward angles and ±15° at backward angles for the incoming and outgoing photon beam. These detectors are 1mm thick on the PiP side and 2mm thick on the opposite side. The outer ring only covered the angles where the detectors ToF 1, ToF 2 and ToF 3 were placed and was 2mm thick. The experiment was triggered on charged particles leaving signals in both rings of start detectors or

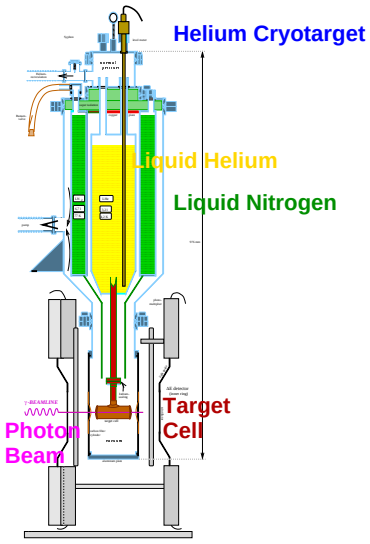

FIG. 7: Schematic diagram of liquid helium target[18].

in the inner ring and PiP. Events were fast cleared if less than two of the six detector systems fired. Thus the experiment measured ^{16}O(γ,pp) events into all pairs of detectors, except ToF 4 and ToF 5, and ^{16}O(γ,pn) events where the proton was detected in ToF 1, ToF 2, ToF 3 or PiP and the neutron was detected in any of the other ToF detectors.

Figure 7 shows a diagram of the cryogenic liquid helium target[18] used in the experiment. The target cell was a cylinder 80 mm long with a diameter of 30 mm made from 200 μm thick Capton foil. The cell was connected to a reservoir of liquid helium at a temperature of 4.2K, which was thermally isolated by a vacuum. Radiation heat input was minimised by the use of super-insulation foil wrappings round the target and by heat shielding maintained at liquid nitrogen temperature. The level of liquid helium was monitored using a resistance thermometer. When the liquid had evaporated to a level just above the target cell the reservoir was refilled. The holding time of the liquid helium target was about 10 hours.

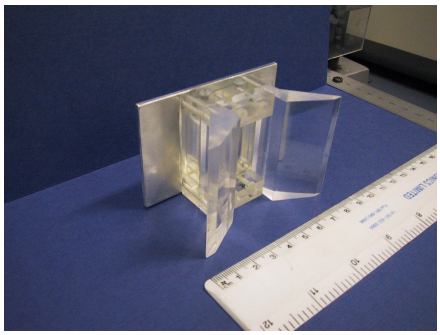

FIG. 8: Photograph of prototype water target.

Fig. 8 shows a prototype of the water target used for the ^{16}O(γ,NN) measurements. The water target was 15mm thick. It consisted of a perspex frame with 50μm Mylar windows at the front

and back. The shaped perspex wings were designed to minimise loss of energy resolution for pairs of protons in PiP and ToF 3. These shapes ensured that the two protons passed through the same total amount of material irrespective of where the reaction took place in the target.

3. DATA ANALYSIS

The calibration of the detectors and the analysis of the experimental data is currently under way. This section shows some of the details of the calibration process.

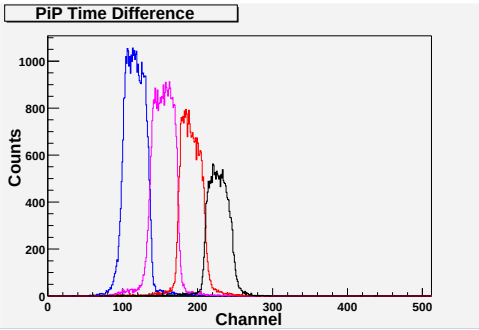

FIG. 9: Time difference spectrum from one PiP horizontal scintillator bar in coincidence with signals from four vertical scintillator strips in front of it.

Fig. 9 illustrates the procedure for the position calibration of PiP. PiP has one layer of thin vertical scintillator strips followed by four layers of thick horizontal scintillator bars. The position in each bar or strip is obtained from the time difference between signals recorded in the photomultiplier tubes at each end. To calibrate the position in each horizontal bar, coincidences are taken with signals in each vertical strip. The figure shows time difference spectra in one horizontal bar gated on coincident signals in each of the four strips in front of it. The points of overlap are clearly defined and form the basis for the calibration. A similar technique is used to calibrate the vertical strips.

Figure 10 illustrates the position calibration of a ToF bar in stand ToF 3. In this case we used a thin scintillator "Paddle" which we placed horizontally in front of, or behind, a stand of ToF bars. A series of measurements was taken with the "Paddle" at different heights on each ToF stand. Again the time difference spectrum from both ends of each ToF bar was gated with signals from the "Paddle" detector. A Gaussian was fitted to the spectrum obtained and the mean time difference was then plotted as a function of position along the bar (see figure 11).

Figure 12 shows a Pulse Height vs. Mean Time spectrum (Sail Plot) for one of the forward ToF bars in stand ToF 4. The pulse height shown is a geometric mean of the signal amplitudes from both ends. Combining the signals from both ends in this way effectively removes any exponential attenuation of pulse amplitudes with position along the bar. The time is an average of signals from both ends which gives a time of arrival of particles at the bar which is independent of position.

The plot is dominated by charged particles, since neutrons only have a detection efficiency of $\sim$5%. The "Sail" outline is the characteristic signal of high energy protons. The rising edge is due to protons, with high energies and short flight times, which pass through the ToF bar and only deposit part of their energy. Lower energy protons, which are stopped in the detector, form the trailing edge of the "Sail". The "Foldback" corresponds to protons of energy 78 MeV which just pass through the bar. This foldback is used to align and calibrate the pulse height response of all the ToF bars in order to facilitate particle identification and allow uniform pulse height thresholds to be set. The "Gamma Flash" arises from relativistic particles and provides a signal which can be used to deduce the true start time of the reaction, which is needed to calibrate the flight times of the detected particles. There is some random background evident in the figure, but this is mainly

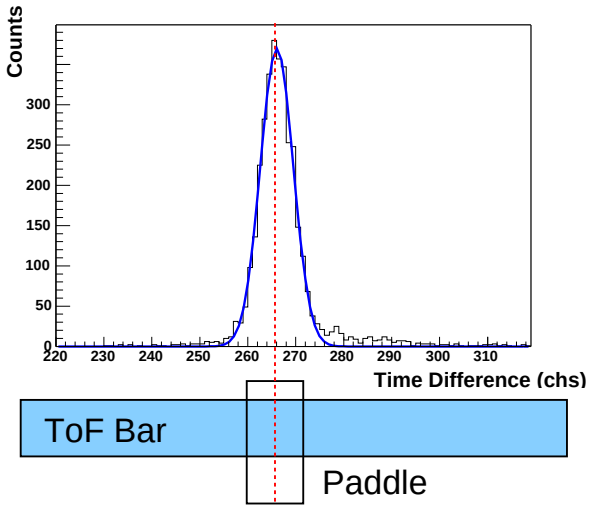

FIG. 10: ToF position calibration using coincidences with a moveable scintillator "Paddle" detector.

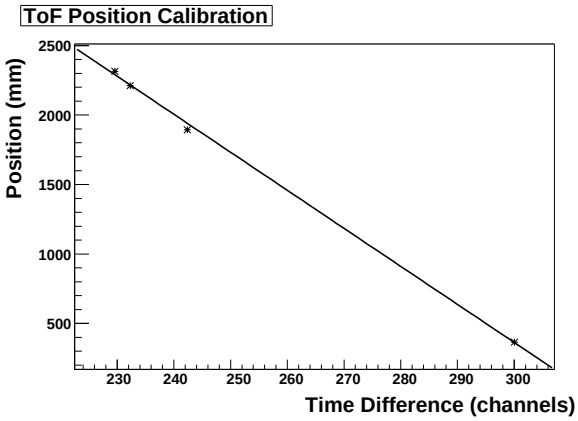

FIG. 11: ToF position vs. time difference graph.

restricted to low pulse amplitudes. It is expected that further improvements in resolution will be obtained by corrections for the residual pulse height attenuation near the ends of the ToF bars. Addition of signals from successive layers should also help to distinguish high energy protons from the low pulse amplitude random background.

4. SUMMARY AND OUTLOOK

(γ,NN) experiments have been carried out on both ^{4}He and ^{16}O nuclei, in near-super parallel kinematics, over a range of photon energies spanning the Δ-resonance and extending significantly above it. These kinematics have been chosen to suppress MEC and Δ-current contributions. For isospin reasons this suppression is expected to be larger for the (γ,pp) channel, than (γ,pn) . However, both reaction channels have been measured and will be analysed. The data obtained are expected to be sensitive to NNCOR and in the (γ,pp) case will provide a test of models of central

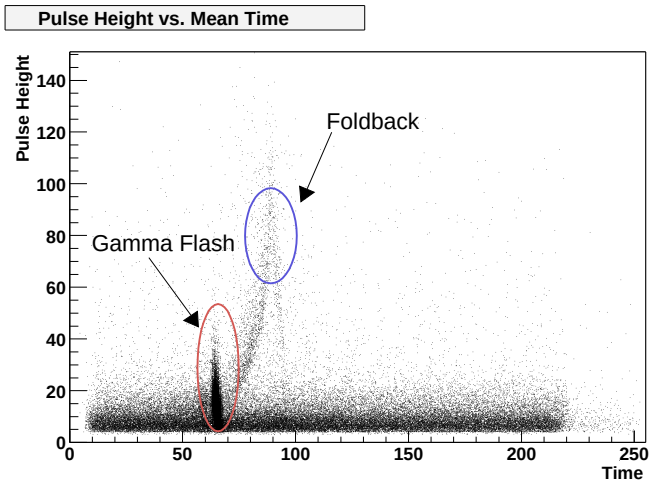

FIG. 12: ToF pulse height vs. mean time of arrival for a ToF bar in stand ToF 4.

SRC.

The data anlysis is underway and definite results should be available in time for the next workshop in this "Two-Hadron Emission" series.

5. ACKNOWLEDGEMENTS

This work has been supported by grants from the UK EPSRC and the German DFG.

[1] J. S. Levinger, Phys. Rev. **84** (1951) 43
[2] K. Gottfried, Nucl. Phys. **5** (1958) 557
[3] S. N. Dancer *et al.*Phys. Rev. Lett. **61** (1988) 1170;
I. J. D. MacGregor *et al.*, Nucl. Phys. **A 533** (1991) 269;
S. M. Doran *et al.*, Nucl. Phys. **A 559** (1993) 347;
J. C. McGeorge *et al.*, Phys. Rev. **C 51** (1995) 1967;
T. Lamparter *et al.*, Z. Phys. **A 355** (1996) 1;
P. Grabmayr *et al.*, Phys. Lett. **B 370** (1996) 17;
P. D. Harty *et al.*, Phys. Lett. **B 380** (1996) 247;
T. T.-H. Yau *et al.*, Eur. Phys. J. **A 1** (1998) 241;
I. J. D. MacGregor *et al.*, Phys. Rev. Lett. **80** (1998) 245;
D. P. Watts *et al.*, Phys. Rev. **C 62** (2000) 014616
[4] D. P. Watts, Ph.D. Thesis, University of Glasgow 1997
[5] R. C. Carrasco and E. Oset, Nucl. Phys. **A 536** (1992) 445;
R. C. Carrasco *et al.*, Nucl. Phys. **A 570** (1994) 701
[6] J. Ryckebusch *et al.*, Phys. Rev. **C 57** (1998) 1318;
J. Ryckebusch *et al.*, Phys. Lett. **B 441** (1998) 1;
L. Machenil *et al.*, Phys. Lett. **B 316** (1993) 17;
J. Ryckebusch *et al.*, Phys. Lett. **B 291** (1992) 213;
J. Ryckebusch *et al.*, Nucl. Phys. **A 568** (1994) 828;
M. Vanderhaegen *et al.*, Nucl. Phys. **A 580** (1994) 551

[7] S. Boffi *et al.*, Electromagnetic Response of Atomic Nuclei, Oxford University press (1996);
C. Giusti *et al.*., Phys. Rev. **C 60** (1999) 054608;
C. Giusti *et al.*, Nucl. Phys. **A 546** (1992) 607;
S. Boffi *et al.*, Nucl. Phys. **A 564** (1993) 473;
C. Giusti and F. D. Pacati, Nucl. Phys. **A 641** (1998) 297;
C. Giusti and F. D. Pacati, Phys. Rev. **C 61** (2000) 054617;
C. Giusti and F. D. Pacati, nucl-th/0102036;
C. Giusti and F. D. Pacati, Nucl. Phys. **A 535** (1991) 573;
C. Giusti and F. D. Pacati, Nucl. Phys. **A 571** (1994) 694
[8] D. Knödler and H. Müther, Phys. Rev. **C 63** (2001) 044602
[9] M. Schwamb *et al.*, Eur. Phys. J. **A 17** (2003) 17;
M. Schwamb *et al.*, nucl-th/0307003;
M. Schwamb, contribution to this workshop
[10] Y. Dewulf *et al.*, Phys. Rev. Lett. **90** (2003) 152502; and refs therein.
[11] P. Grabmayr *et al.*, Mainz PAC Proposal A1/4-98 (1998)
[12] E. Jans *et al.*, Mainz PAC Proposal A1/5-98 (1998);
E. Jans and P. Barneo, contribution to this workshop
[13] G. Orlandini and L. Sarra, in Proc. of the Second Workshop on Electromagnetically Induced Two-Nucleon Emission, eds. J. Ryckebusch and M. Waroquier, Gent (1995) p. 1
[14] I. Anthony *et al.*, Nucl. Inst. Meth. Phys. Res. **A 301** (1991) 230;
S. J. Hall *et al.*, Nucl. Inst. Meth. Phys. Res. **A 368** (1996) 698
[15] H Herminghaus , Proc. Linear Accelerator Conf., Albuquerque, NM, 1990;
T. Walcher, Prog. Part. Nucl. Phys. **24** (1990) 189
[16] P. Grabmayr *et al.*, Nucl. Inst. Meth. Phys. Res. **A 402** (1998) 85
[17] I. J. D. MacGregor *et al.*, Nucl. Inst. Meth. Phys. Res. **A 382** (1996) 479
[18] S. Oberkirsch, Diplomarbeit, Universität Tübingen (1996)
[19] J. Leypold, Diplomarbeit, Universität Tübingen (1994);
A. Settle, Diplomarbeit, Universität Tübingen (1996)